catalysts

MDPI

Article

Facile and Novel Route for the Preparation of ZnO Nanoparticles with Different Cr Loadings for Opto-Photocatalysis Applications

Tahani M. Bawazeer

Department of Chemistry, Faculty of Applied Science, Umm Al-Qura University, Makkah 21955, Saudi Arabia; tmbawazeer@uqu.edu.sa; Tel.: +966-5-5559-5399

Abstract: The current article deals with the facile yet novel route to prepare zinc oxide (ZnO) nanoparticles with different weight percentages of chromium as a dopant. The impact of such dopant into the ZnO host lattice is explored in terms of the structural, vibrational, optical, and photocatalytic characteristics. The Bragg reflections in the X-ray diffraction displayed a phase pure wurtzite ZnO hexagonal system. The morphology reflects spherical-shaped ZnO particles in all the systems. The optical analysis ensured a good ultraviolet light absorption and a bandgap energy in the range of 3.30–3.24 eV. The principal Raman vibrations ensured the presence of the wurtzite ZnO crystal structure. The decolorization experiment of methyl green dye with pristine and various chromium-doped ZnO nanoparticles was conducted under the illumination of visible light. The obtained results showed that the incorporation of Cr in the framework significantly improved the photocatalytic performance of ZnO.

Keywords: photocatalysis; ZnO; Cr; doping; activity; water treatment

Citation: Bawazeer, T.M. Facile and Novel Route for the Preparation of ZnO Nanoparticles with Different Cr Loadings for Opto-Photocatalysis Applications. *Catalysts* **2022**, *12*, 1093. https://doi.org/10.3390/catal12101093

Received: 31 August 2022
Accepted: 19 September 2022
Published: 21 September 2022

1. Introduction

Sun radiant heat or light is the most common clean energy source available in today's world. It is a stupendous fact that the amount of solar radiation that hits the earth's surface in an hour is greater than the energy consumption over the course of a year. As a result, the research across the globe is intensified towards the development of materials to harvest solar irradiation and energy conversion. Besides the photovoltaic or solar cell, the solar energy can be utilized to eliminate environmental hazards with the photocatalytic mechanism. In this way, a photocatalysis uses the clean solar energy to spearhead the chemical reactions through redox (oxidation and reduction) reactions to degrade organic pollutants [1–3]. Thus, the method has garnered the scientific community's interest to consider it as the most promising tool to handle environmental concerns, in particular wastewater treatment.

Photocatalysis is a photochemical reaction at the surface of a semiconductor in which two simulation reactions occur, the first involves oxidation from photoinduced positive holes and the second is reduction from photo-induced electrons. On the other hand, advances in nanoscience and technology have made for the development of new ways to clean up polluted water possible. In this way, nanoparticles are studied all over the world for their better surface and interface properties compared to their bulk form upon their tuneable shape and size. In such trials, the researchers are keen to work with transition metal-oxide nanostructures in optoelectronic applications for their tuneable bandgap. The promising light-driven properties of well-known metal oxides such as titanium dioxide (TiO_2) [4–6], zinc oxide (ZnO) [7,8], iron (III) oxide (Fe_2O_3) [9,10], zirconia (ZrO_2) [11,12], copper oxide (CuO) [13], and tungsten trioxide (WO_3) [14] were employed as photocatalysts. Besides the promising photocatalytic behavior, each material has its own pros and cons.

Zinc oxide (ZnO) is a well-established semiconductor with its non-toxic, cost effective, and scaled up preparatory methods [8,15–17]. The wide direct bandgap (3.2–3.4 eV) and the ability to fine-tune its properties alongside the high binding energy of ~60 meV at room temperature make it interesting amongst the metal oxide nanostructures. Besides these attractive qualities, the high chemical stability, high surface reactive nature, photonic excitonic and good photosensitive nature upholds its investigations in photocatalytic reactions. However, the pristine ZnO has a relatively faster recombination rate due to its wide bandgap (UV region) and low quantum efficiency. In other words, the large bandgap can be addressed as its transparent nature in the visible region. Such undesired qualities hinder its practical ability to serve as a photocatalyst to degrade targeted pollutants.

To address these limitations, one of the promising ways is the doping of transition metals (TMs) into the ZnO photocatalyst. In such ambition, various TMs such as the copper (Cu), cobalt (Co), nickel (Ni), and silver (Ag) are inserted into the host lattice for the improvement of its applications [18–23]. Besides these metal dopants, chromium (Cr) has its due importance for the close resemblance of host Zn atoms in many aspects [24–28]. The Cr^{3+} (0.65 Å) has a smaller ionic radius as than the host Zn^{2+} (0.74 Å) while the other possible Cr^{2+} (0.73 Å) is identical to the host. This may allow the Cr dopant to easily infiltrate the ZnO crystal lattice or could replace the Zn atom's position in the crystal system. This enables the Cr dopant to successfully induce lattice defects and alter the surface area of the host ZnO system. Beside this prominent role, the Cr-doped ZnO has an intriguing property of chemisorption of O_2 at the Cr site, which allows Cr-doped ZnO to effectively control the band gap and improve charge carrier separation. It makes the doping process easier and insertion of Cr into the ZnO lattice is feasible. This makes the Cr dopant and ZnO host promising materials in adsorption and catalytic applications. In the pursuit of such alterations of the ZnO host lattice, investigations on a Cr-doped ZnO system for opto-electronic applications are carried out.

Methyl green is a dye which is continuous in the environment due to its wide utilization in domestic products such as leather, clothing, etc. It is toxic to most aquatic and terrestrial living organisms. It is alarming and deadly to freshwater fishes upon acute and chronic exposure. The clinical models and their findings revealed that MG dye is a multiple-organ toxin. It hinders the food intake, growth, and fertility rates besides damaging the major organs such as the spleen, liver, kidney, heart, and sensory organs. The investigation of MG exposure in animals indicates that it is highly toxic to mammalian cells and served as the growth factor of tumors in the lungs, breast, and ovaries. It implies that it is proved to be a respiratory enzyme toxin. Periodic exposure to the MG dye causes anemia, leukocytosis (increased WBC condition), and poor blood clotting [29,30]. In summary, the dye poses an environmental threat to countries across the globe and was chosen for photocatalytic degradation experiment. Thus, an attempt to prepare pristine ZnO and to dope different weight percentages of Cr into the ZnO system was undertaken. The prepared nanoparticles were taken as a photocatalyst for the decolorization of methyl green dye and the best performing system was examined for reusability.

2. Experimental Details

2.1. Synthesis

The synthesis of the prepared photocatalysts (the bare ZnO and the Cr-doped ZnO samples) proceeded through a one-step flash combustion method. In this method, three simple steps are involved which are mixing, drying, and finally calcination. In the real synthesis, 5 g zinc nitrate hexahydrate +0.5 g citric acid +2 mL acetone were used and mixed and dried at 100 °C for 24 h. In similar way the other 4 samples were prepared with 1.0, 2.5, 5.0, and 7.5 wt.% of chromium nitrate nonahydrate as the Cr-doping source. After drying and mixing, all samples were inserted inside the furnace at 550 °C for 3.30 h.

2.2. Characterizations

The prepared nanoparticles were subjected to various characterization tools. The X-ray diffractometer was used to extract the structural properties of the prepared nanoparticles. The vibrational analysis was carried out with the aid of a Raman spectrometer. UV-DRS spectroscopy was used to measure the optical reflectance and its subsequent parameters were estimated. The morphology was captured by using a scanning electron microscope.

2.3. Photocatalytic Performance Investigation

The photocatalytic experiment was carried out in a photoreactor equipped with a visible light lamp which can emit several wavelengths in the visible light region, however, the majority are centered at 425 nm. The decolorization of methyl green (MG) was chosen as a model reaction to study the photocatalytic performance of the prepared photocatalysts. In a real experiment, 50 mL of aqueous MG solution were mixed with 0.1 g of the catalyst sample and the overall mixture as ultrasonicated in a dark box for 30 min. After that, the mixture was moved to the photoreactor and the samples were withdrawn at time intervals, filtrated to remove the catalyst sample, and the color intensity of the dye solution was measured with a spectrometer in the range between 300 and 800 nm.

3. Results and Discussion

3.1. Structural Analysis

The XRD diffraction pattern of the as-prepared and various Cr-doped zinc oxide nanoparticles is displayed in Figure 1A. The pristine zinc oxide system replicates a phase pure wurtzite hexagonal crystal system of ZnO material. The Bragg reflections are ascribed to (101), (002), (101), (102), (110), (103), and (112) as listed in JCPDS card no 36–1441. The peaks are intense and exhibit good crystalline nature. In addition, there are no diffraction peaks contributing to defects or other phases of ZnO. The X-ray diffraction pattern of Cr-doped ZnO systems is displayed in the Figure 1A. The insertion of Cr as a dopant did not lead to any additional peaks or new phases in the system. This implies that the complete insertion of Cr as a dopant does not form separate phases and paves the way for notable dispersion into the system. The peak positions of the wurtzite ZnO system is also not considerably disturbed upon doping Cr into the crystal lattice in a chronological order. Taking this analysis into account, the following arguments could be made: the doped Cr atoms could replace the host Zn atoms in the crystal lattice since the ionic radii of Cr^{3+} (0.65 Å) is smaller than the host Zn^{2+} (0.74 Å) while the other possible Cr^{2+} (0.73 Å) [31] is almost identical to the former. The diffraction peaks shifted toward higher angles when some Zn^{2+} (0.74 Å) were replaced with smaller Cr^{3+} dopants as visible from Figure 1A(b), which is in accordance with an earlier report [31].

Williamson–Hall (W-H) analysis is a facile integral method which accounts for peak broadening induced by crystallite size and lattice strain as a function of diffraction angle 2θ [32]. The W-H plots of βcosθ vs. 4sinθ were plotted against each other and linear fit was constructed as illustrated in Figure 1B(a–e). The intercept on the y-axis was utilized to estimate the crystallite size while the slope was used to measure the lattice strain. The crystallite size of the prepared ZnO and Cr-doped ZnO systems was estimated using the relation

$$D_{ave} = \frac{k\,\lambda}{\beta\cos\theta} \quad (1)$$

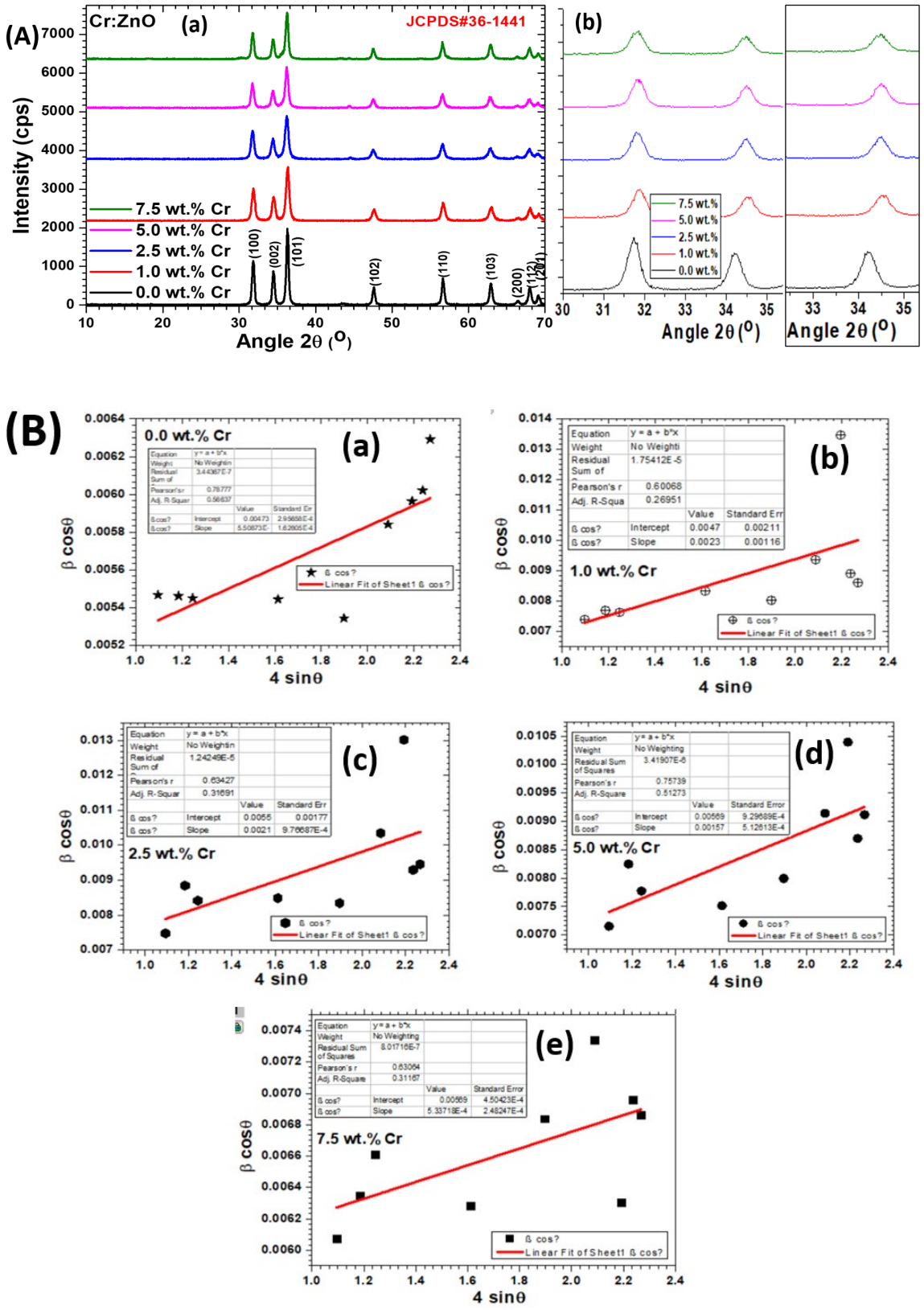

Figure 1. (**A**) (**a**) XRD patterns and (**b**) close view of the peak shift for pure and Cr-doped ZnO NPs. (**B**) W-H plots for (**a**) pure and (**b**–**e**) Cr-doped ZnO NPs.

The estimated values are listed in Table 1. The average crystallite size for the pristine ZnO system was estimated as 29.32 nm. The 1.0 wt.% doped system displayed a slight decline in crystallite size implying the broadening of the peak. The trend continued until the maximum Cr-doped system had an average crystallite size of 23.86 nm. Such behavior can be linked to the decrease in intensity of the peaks indicating the loss in crystallinity due to lattice distortion. Henceforth, the dopant Cr could be incorporated into the host ZnO lattice sites instead of its interstitial sites. The strain is assumed to be isotropic in the W-H model. It will be the same in all crystallographic planes and considered as the uniform deformation model used (UDM). The strain values increased with the increase in dopant concentrations of chromium. It implied the reduction of crystallinity with the dislocation density (lines/m^2) estimated, as reported elsewhere. The analysis confirmed that the Cr as a dopant is successfully inserted into the ZnO lattice without forming any new composition or defect phases.

Table 1. The W-H plot microstructural parameters determined for pure and Cr-doped ZnO NPs.

Samples	D (nm)	Dislocation Density (lines/m^2)	ε ($\times 10^{-3}$)
0.0 wt.%	29.31298	1.18×10^{15}	0.55
1.0 wt.%	28.9458	1.27×10^{15}	2.31
2.0 wt.%	24.89235	1.61×10^{15}	2.12
3.0 wt.%	24.19728	1.70×10^{15}	1.57
5.0 wt.%	23.8641	1.75×10^{15}	0.53

3.2. Vibrational Analysis

Raman spectroscopy is an efficient tool to investigate the semiconductor ZnO nanoparticles and impact of Cr as a dopant in the ZnO lattice. The Raman active modes for a ZnO wurtzite crystal structure can be represented as $A_1 + E_1 + 2E_2$ in which A_1 and E_1 correspond to polar phonons while the E_2 symmetry is non-polar. The polar phonon modes can be classified into transverse optical (TO) and longitudinal-optical (LO) phonons. On the other hand, the non-polar mode is ascribed to high and low wavenumbers associated with the oxygen atoms and Zn sublattices [33]. In such aspirations, the Raman spectra for the pristine ZnO and Cr-doped ZnO structures are recorded as the function of wavenumber in the region of 100–1400 cm^{-1} as displayed in Figure 2. The undoped ZnO nanoparticles displayed characteristics peaks of ZnO without any impure phases [34]. The prominent peaks at 108 and 436 cm^{-1} corresponding to E_2 (low) and E_2 (high) affirmed the wurtzite phase of ZnO as reported in the XRD analysis. In the Cr-doped systems, the intensity of all the peaks is diminished macroscopically. Such behavior can be related to the occupancy of Cr ions in the place of Zn atoms in the sublattice which perturbs the lattice arrangement. In addition, the change can be linked to the lattice distortions created by the insertion of Cr in the place of Zn in the sublattices. The second order Raman vibrations are seen at 332 cm^{-1} which is generated by the zone boundary phonon scattering. The peak around 582 cm^{-1} is assigned to the LO mode E_1 symmetry indicating that the c-axis of the wurtzite is perpendicular to the surface. A few new peaks in the range of 800–1200 cm^{-1} came into existence upon the insertion of Cr dopant into the ZnO lattice [35,36]. It can be attributed to the structural defects, crystallite size, microstrain, and lattice defects upon increasing dopant concentrations. The Raman analysis concluded that the Cr dopant was successfully inserted into the host lattice without forming any new phases and suppressed the primary vibration's intensity but not the primary peak positions.

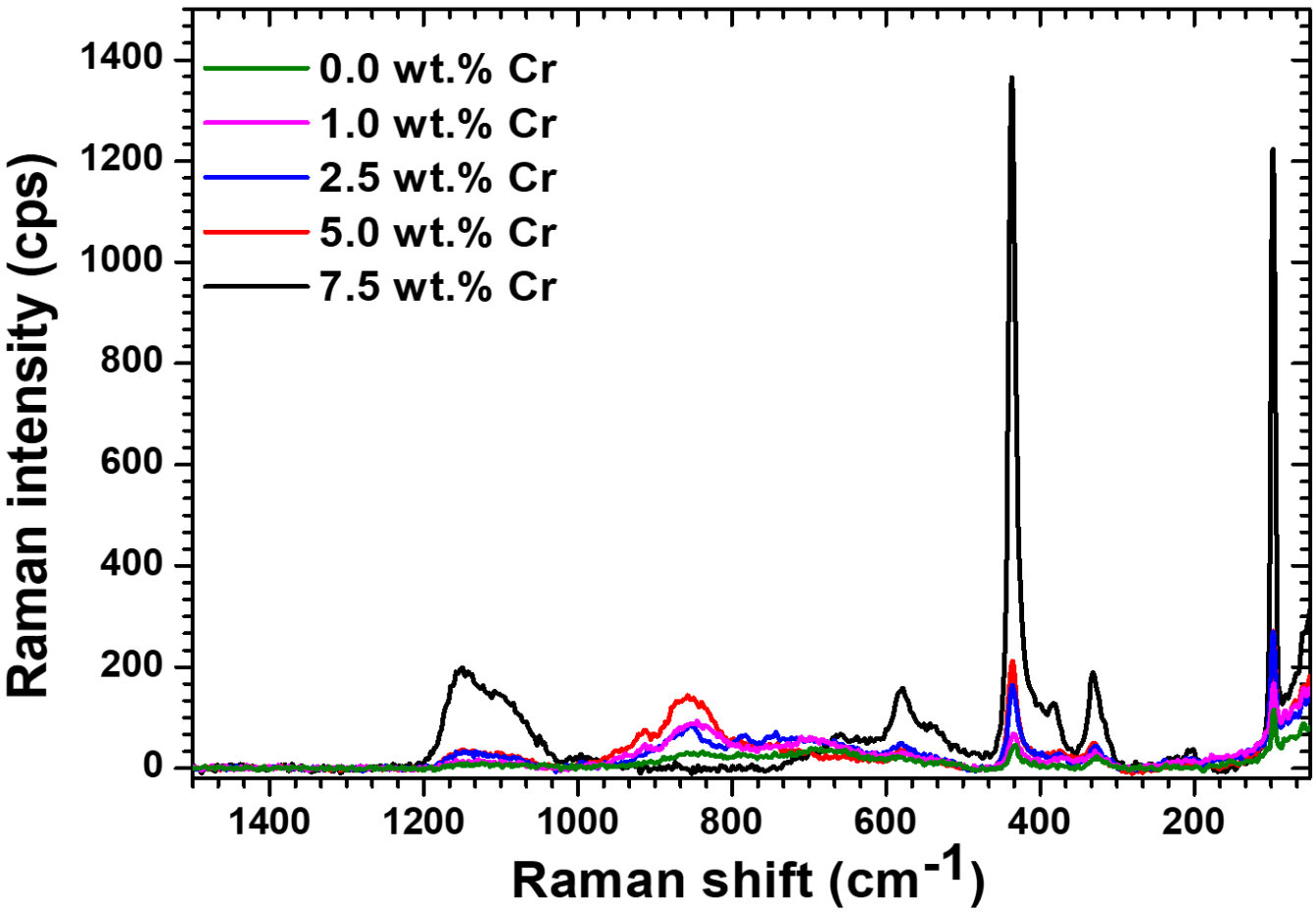

Figure 2. Raman spectra for pure and Cr-doped ZnO NPs.

3.3. Morphological Analysis

The morphological features of the pristine ZnO and various Cr wt.% doped ZnO systems were recorded in the scale of 500 nm and displayed in Figure 3. The pristine ZnO morphology depicts spherical-shaped ZnO particles with a high mono-dispersed nature. As discussed in the XRD analysis, the crystallite size decreased upon increasing dopant concentrations. It is reflected in the morphological features. Despite the agglomeration in the lower dopant concentrations, the particle size is smaller than the pure ZnO system. It suggests that the inserted Cr plays a significant role in nucleation and hinders the growth mechanism of ZnO particles. As the dopant concentration increases the agglomeration of particles is reduced in the macroscopic view. The particles are distinct and closely packed without many grain boundaries. This leads us to conclude that the Cr ions are strongly absorbed into the system which prevented the agglomeration of particles with the steric hindrance effect. The reduced particle size and good crystalline nature of highest doped ZnO system reflects the optical and photocatalytic experiments. This is in agreement with the XRD results which were discussed earlier.

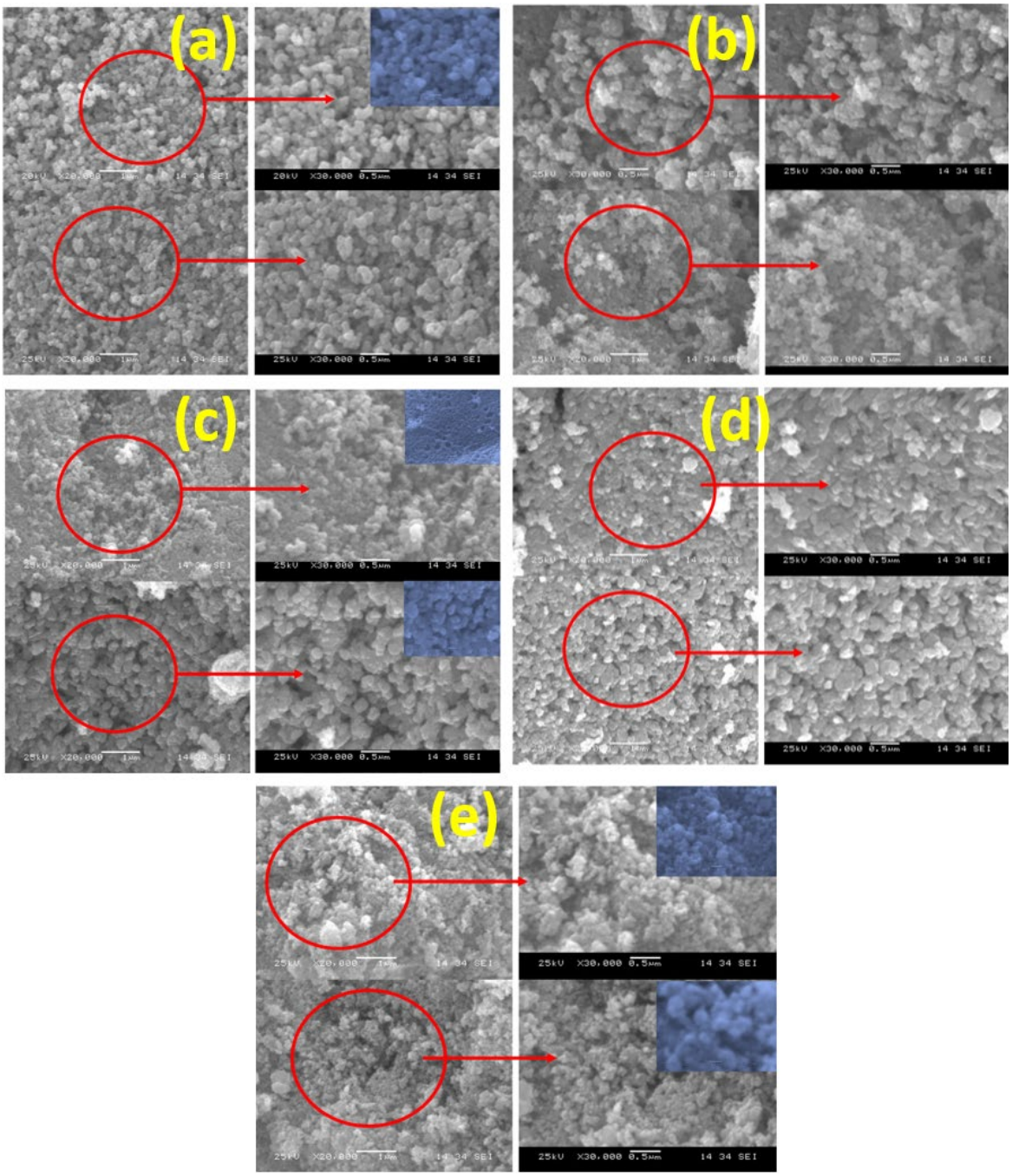

Figure 3. SEM images for (**a**) pure and (**b**–**e**) Cr-doped ZnO NPs.

3.4. Optical Energy Gap Analysis

The reflectance measurements were taken in the 200–800 nm wavelength range and are shown in Figure 4a. Among the prepared materials, the undoped ZnO nanoparticles have the highest reflectivity in the visible area. When doping is used, the reflectance behavior is greatly decreased when compared to the pure material. Furthermore, when Cr is added to the host lattice, the absorption margins of ZnO nanoparticles were altered compared to the bare sample. It means that the band energy of ZnO nanoparticles was modified. The Kubelka–Munk function, which represents the linear absorption coefficient F(R), can be estimated by using the relation

$$F(R) = (1 - R)^2/2R \quad (2)$$

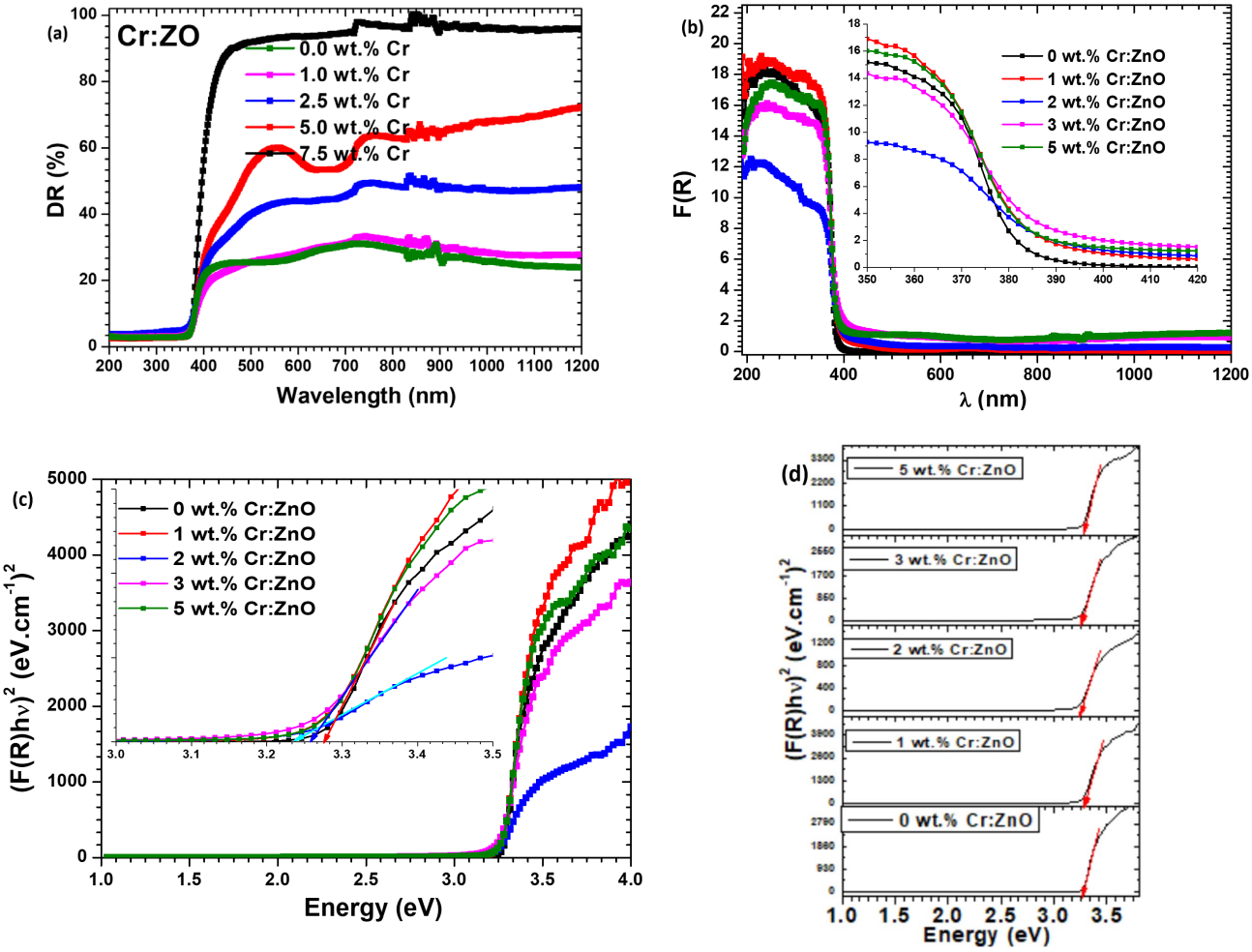

Figure 4. (**a**) DR, (**b**) Kubelka–Munk function, (**c**) energy gap plots, and (**d**) band gap plots separately for pure and Cr-doped ZnO NPs.

The estimated values, as shown in Figure 4b, indicate that the prepared ZnO particles with different dopant concentrations of Cr have a good absorption in the 300–380 nm wavelength region of the spectrum with a cut-off wavelength of 400 nm. Additionally, the reduced crystallite size induces a redshift in the absorbance features upon increasing dopant concentrations. This is evident with absorption onset shifted towards the visible region of the EM spectrum and has an impact on bandgap of the prepared materials. The bandgap of the pristine and Cr-doped ZnO nanoparticles is calculated using the Kulbeka–Munk relation which is expressed in terms of the Tauc relation as

$$(F(R)h\upsilon)^2 = A(h\upsilon - Eg) \quad (3)$$

where the terms used in the equation represent the same meanings as reported elsewhere. The photoenergy (hν) on the x axis is plotted against the $(F(R)h\nu)^2$ on the *y* axis. The extrapolation at x = 0 provides the optical bandgap of the prepared nanomaterials as shown in Figure 4c. The pristine ZnO nanoparticles have a bandgap of 3.27 eV and the bandgap values shift to the lower side upon the insertion of Cr into the host lattice. Since there are no drastic changes in the crystallite size (Δ7 nm), the dopant initiated a small growth inhibition in the host lattice. Thus, the changes in the bandgap of the ZnO semiconductor are also on a smaller scale. As discussed earlier, the redshift in the system was reflected in the bandgap values upon various dopant concentrations of Cr ions. Such substitution shifted the bandgap to the lower values by creating extra energy levels in the bandgap of the host ZnO near its valence and conduction bands. It takes accountability for the

narrowed bandgap upon increasing dopant concentrations by forming the sub-band states. Such behavior could be linked to the dopant-created vacancies in the ZnO crystal lattice. The drop in bandgap energy is attributed to altered crystallite size, lattice defects, and dopant induced strain in the crystal lattice.

3.5. Photocatalysis Analysis

As mentioned in the introduction, methyl green (MG) dye was chosen for the photocatalytic experiments. The decolorization of a dye via photocatalysis can be accomplished using the following mechanism: during the exposure of the semiconductor catalyst to ultraviolet radiation, the electrons in the valence band become excited and reach the conduction band which in turn forms an exciton (electron-hole pair). The generated hole and electron can move around the catalyst surface and initiate the redox reaction with the species existing on the surface.

In general, the holes in the valence band react readily with the surface-bound water molecules and produce OH radicals. On the other hand, the electrons in the conduction band react with the oxygen molecules to develop a superoxide radical anion of oxygen. Such reactions block the recombination mechanism of an electron and the hole which are generated as the first product. It eventually paves the way to form other species and accounts for the decolorization/degradation of dye molecules. Thus, the photocatalytic decomposition of dyes is considered as a liable method to treat industrial waste. In the current case, the methyl green (MG) dye was mixed with pristine ZnO and Cr-doped ZnO semiconductor catalysts for a decolorization test as a function of time (60 min). The time-dependent decolorization of the MG dye is illustrated in Figure 5a. The decolorization of the dye is maximum when it is mixed with 7.5 wt.% of Cr as a dopant in the ZnO system. This implies that the dopant at the highest level can hinder the recombination rate and acts as a charge carrier separator in the ZnO system. Similar outcomes were reported earlier by Chang et al. [37]. This could be linked to the change in crystallite size, microstrain, and altered optical properties. In summary, the above-mentioned catalyst decolored 90% of the dye solution in 60 min.

The pseudo first-order kinetics were carried out as a function of time under the visible light irradiation with pristine ZnO and the Cr-doped system as the reaction catalyst. The Langmuir Hinshelwood kinetics [37] were used to examine the kinetics of photodegradation of the MG dye with the relation as reported elsewhere

$$In\left(\frac{C}{C_o}\right) = -kt \tag{4}$$

where k is the kinetic rate constant for MG dye degradation (min^{-1}), represented by the slope of the $ln(C/C_o)$ vs. t graph, t is the irradiation period (minutes), and C_o and C are the initial and final concentrations (Molar), respectively. The linear behavior of the catalyst ensures that the system follows the first-order kinetics. The rate constants of pristine and various Cr-doped ZnO catalysts are displayed in Figure 5c. A few experiments were repeated to study the repeatability of the obtained results. Almost similar results were observed with a small experimental error (not more than 4%) which shows the high reproducibility of the obtained results. The better performance of the highest doped system was taken for the reusability test and the results gave promising signs to serve as a stable photocatalyst.

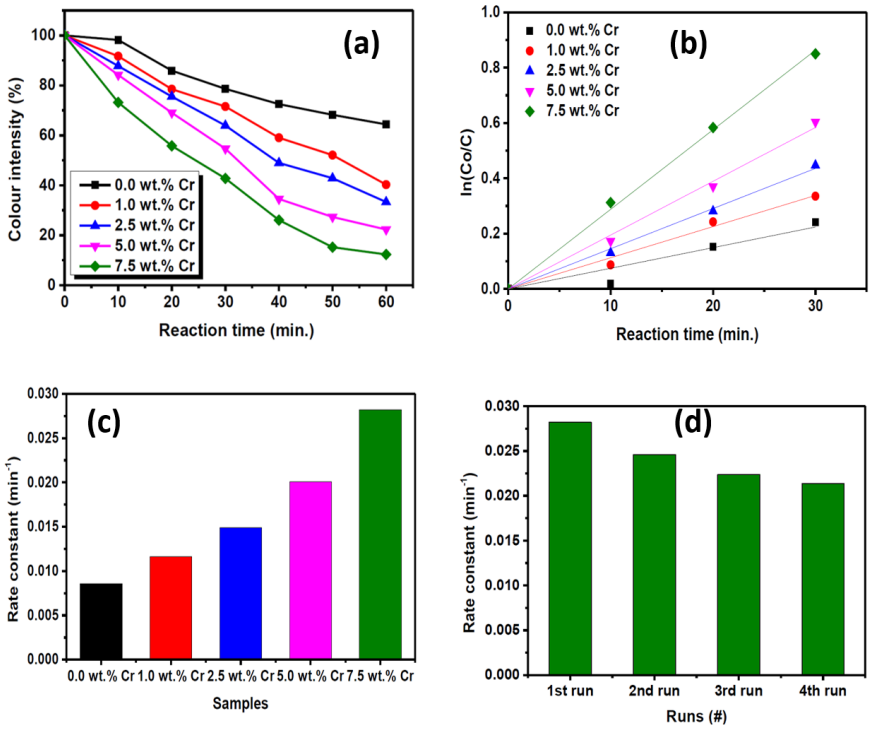

Figure 5. (**a**) The change in MG concentration during the photocatalysis experiments over the prepared Cr-doped ZnO samples, (**b**) the pseudo first-order kinetic model of the photocatalytic experiments, (**c**) the calculated rate constants of the prepared samples, and (**d**) the reusability investigation of the prepared 7.5 wt.% Cr sample.

4. Conclusions

Zinc oxide nanoparticles and different weight percentages of chromium dopant into the ZnO system were successfully prepared with a facile coprecipitation method. The structural properties of the pristine and Cr-doped ZnO system revealed a replica of the hexagonal wurtzite ZnO crystal structure. It was duly supported by the principal Raman vibrations corresponding to the above-mentioned phase. The optical properties of the prepared ZnO nanoparticles revealed that it has a strong absorption in the UV region with a bandgap of around 3.3 eV. The methyl green dye was used for the decolorization test with the prepared samples as a photocatalyst. It followed the first order kinetics with the linear behavior. The highest doped ZnO system showed superior decolorization with around 90% of MG degradation. It showed promising signs in the reusability test and can be used for future experiments.

Funding: This research received no external funding.

Data Availability Statement: The data presented in this study are available on request from the author. The data are not publicly available due to privacy issues.

Conflicts of Interest: The author declares no conflict of interest.

References

1. Ameta, R.; Solanki, M.S.; Benjamin, S.; Ameta, S.C. Photocatalysis. In *Advanced Oxidation Processes for Waste Water Treatment: Emerging Green Chemical Technology*; Academic Press: Cambridge, MA, USA, 2018; pp. 135–175. [CrossRef]
2. Bahnemann, D. Photocatalytic water treatment: Solar energy applications. *Sol. Energy* **2004**, *77*, 445–459. [CrossRef]
3. Ravelli, D.; Dondi, D.; Fagnoni, M.; Albini, A. Photocatalysis. A multi-faceted concept for green chemistry. *Chem. Soc. Rev.* **2009**, *38*, 1999–2011. [CrossRef]
4. Guo, Q.; Zhou, C.; Ma, Z.; Yang, X. Fundamentals of TiO2 Photocatalysis: Concepts, Mechanisms, and Challenges. *Adv. Mater.* **2019**, *31*, 1901997. [CrossRef] [PubMed]

5. Schneider, J.; Matsuoka, M.; Takeuchi, M.; Zhang, J.; Horiuchi, Y.; Anpo, M.; Bahnemann, D.W. Understanding TiO2 Photocatalysis: Mechanisms and Materials. *Chem. Rev.* **2014**, *114*, 9919–9986. [CrossRef] [PubMed]
6. Chen, B.; Meng, Y.; Sha, J.; Zhong, C.; Hu, W.; Zhao, N. Preparation of MoS_2/TiO_2 based nanocomposites for photocatalysis and rechargeable batteries: Progress, challenges, and perspective. *Nanoscale* **2017**, *10*, 34–68. [CrossRef] [PubMed]
7. Ong, C.B.; Ng, L.Y.; Mohammad, A.W. A review of ZnO nanoparticles as solar photocatalysts: Synthesis, mechanisms and applications, Renew. *Sustain. Energy Rev.* **2018**, *81*, 536–551. [CrossRef]
8. Weldegebrieal, G.K. Synthesis method, antibacterial and photocatalytic activity of ZnO nanoparticles for azo dyes in wastewater treatment: A review. *Inorg. Chem. Commun.* **2020**, *120*, 108140. [CrossRef]
9. Hitam, C.N.C.; Jalil, A.A. A review on exploration of Fe2O3 photocatalyst towards degradation of dyes and organic contaminants. *J. Environ. Manag.* **2020**, *258*, 110050. [CrossRef]
10. Mishra, M.; Chun, D.M. α-Fe_2O_3 as a photocatalytic material: A review. *Appl. Catal. A Gen.* **2015**, *498*, 126–141. [CrossRef]
11. Suresh, P.; Vijaya, J.J.; Kennedy, L.J. Photocatalytic degradation of textile-dyeing wastewater by using a microwave combustion-synthesized zirconium oxide supported activated carbon. *Mater. Sci. Semicond. Process.* **2014**, *27*, 482–493. [CrossRef]
12. Selvam, N.C.S.; Manikandan, A.; Kennedy, L.J.; Vijaya, J.J. Comparative investigation of zirconium oxide (ZrO_2) nano and microstructures for structural, optical and photocatalytic properties. *J. Colloid Interface Sci.* **2013**, *389*, 91–98. [CrossRef]
13. Scuderi, V.; Amiard, G.; Boninelli, S.; Scalese, S.; Miritello, M.; Sberna, P.M.; Impellizzeri, G.; Privitera, V. Photocatalytic activity of CuO and Cu_2O nanowires. *Mater. Sci. Semicond. Process.* **2016**, *42*, 89–93. [CrossRef]
14. Quan, H.; Gao, Y.; Wang, W. Tungsten oxide-based visible light-driven photocatalysts: Crystal and electronic structures and strategies for photocatalytic efficiency enhancement. *Inorg. Chem. Front.* **2020**, *7*, 817–838. [CrossRef]
15. Kahouli, M.; Barhoumi, A.; Bouzid, A.; Al-Hajry, A.; Guermazi, S. Structural and optical properties of ZnO nanoparticles prepared by direct precipitation method. *Superlattices Microstruct.* **2015**, *85*, 7–23. [CrossRef]
16. Kumar, S.S.; Venkateswarlu, P.; Rao, V.R.; Rao, G.N. Synthesis, characterization and optical properties of zinc oxide nanoparticles. *Int. Nano Lett.* **2013**, *3*, 30. [CrossRef]
17. Faisal, S.; Jan, H.; Shah, S.A.; Shah, S.; Khan, A.; Akbar, M.T.; Rizwan, M.; Jan, F.; Wajidullah; Akhtar, N.; et al. Green Synthesis of Zinc Oxide (ZnO) Nanoparticles Using Aqueous Fruit Extracts of Myristica fragrans: Their Characterizations and Biological and Environmental Applications. *ACS Omega* **2021**, *6*, 9709–9722. [CrossRef] [PubMed]
18. Kumar, P.; Kumar, A.; Rizvi, M.A.; Moosvi, S.K.; Krishnan, V.; Duvenhage, M.M.; Roos, W.D.; Swart, H.C. Surface, optical and photocatalytic properties of Rb doped ZnO nanoparticles. *Appl. Surf. Sci.* **2020**, *514*, 145930. [CrossRef]
19. Pascariu, P.; Tudose, I.V.; Suchea, M.; Koudoumas, E.; Fifere, N.; Airinei, A. Preparation and characterization of Ni, Co doped ZnO nanoparticles for photocatalytic applications. *Appl. Surf. Sci.* **2018**, *448*, 481–488. [CrossRef]
20. Siva, N.; Sakthi, D.; Ragupathy, S.; Arun, V.; Kannadasan, N. Synthesis, structural, optical and photocatalytic behavior of Sn doped ZnO nanoparticles. *Mater. Sci. Eng. B.* **2020**, *253*, 114497. [CrossRef]
21. Qi, K.; Xing, X.; Zada, A.; Li, M.; Wang, Q.; Liu, S.y.; Lin, H.; Wang, G. Transition metal doped ZnO nanoparticles with enhanced photocatalytic and antibacterial performances: Experimental and DFT studies. *Ceram. Int.* **2020**, *46*, 1494–1502. [CrossRef]
22. Bhargava, R.; Sharma, P.K.; Dutta, R.K.; Kumar, S.; Pandey, A.C.; Kumar, N. Influence of Co-doping on the thermal, structural, and optical properties of sol–gel derived ZnO nanoparticles. *Mater. Chem. Phys.* **2010**, *120*, 393–398. [CrossRef]
23. Tolossa, W.K.; Shibeshi, P.T. Structural, optical and enhanced antibacterial activities of ZnO and (Co, Fe) co-doped ZnO nanoparticles by sol-gel combustion method. *Chem. Phys. Lett.* **2022**, *795*, 139519. [CrossRef]
24. Meng, A.; Xing, J.; Li, Z.; Li, Q. Cr-Doped ZnO Nanoparticles: Synthesis, Characterization, Adsorption Property, and Recyclability. *ACS Appl. Mater. Interfaces* **2015**, *7*, 27449–27457. [CrossRef] [PubMed]
25. Vijayalakshmi, K.; Sivaraj, D. Enhanced antibacterial activity of Cr doped ZnO nanorods synthesized using microwave processing. *RSC Adv.* **2015**, *5*, 68461–68469. [CrossRef]
26. Singh, P.; Kumar, R.; Singh, R.K. Progress on Transition Metal-Doped ZnO Nanoparticles and Its Application. *Ind. Eng. Chem. Res.* **2019**, *58*, 17130–17163. [CrossRef]
27. Hassan, M.M.; Khan, W.; Azam, A.; Naqvi, A.H. Influence of Cr incorporation on structural, dielectric and optical properties of ZnO nanoparticles. *J. Ind. Eng. Chem.* **2015**, *21*, 283–291. [CrossRef]
28. Alkallas, F.H.; Trabelsi, A.B.G.; Nasser, R.; Fernandez, S.; Song, J.M.; Elhouichet, H. Promising Cr-Doped ZnO Nanorods for Photocatalytic Degradation Facing Pollution. *Appl. Sci.* **2022**, *12*, 34. [CrossRef]
29. Srivastava, S.; Sinha, R.; Roy, D. Toxicological effects of malachite green. *Aquat. Toxicol.* **2004**, *66*, 319–329. [CrossRef]
30. Wu, C.; Shen, L.; Zhang, Y.C.; Huang, Q. Solvothermal synthesis of Cr-doped ZnO nanowires with visible light-driven photocatalytic activity. *Mater. Lett.* **2011**, *65*, 1794–1796. [CrossRef]
31. Liu, Y.; Yang, J.; Guan, Q.; Yang, L.; Zhang, Y.; Wang, Y.; Feng, B.; Cao, J.; Liu, X.; Yang, Y.; et al. Effects of Cr-doping on the optical and magnetic properties in ZnO nanoparticles prepared by sol–gel method. *J. Alloys Compd.* **2009**, *486*, 835–838. [CrossRef]
32. Devesa, S.; Rooney, A.P.; Graça, M.P.; Cooper, D.; Costa, L.C. Williamson-hall analysis in estimation of crystallite size and lattice strain in $Bi_{1.34}Fe_{0.66}Nb_{1.34}O_{6.35}$ prepared by the sol-gel method. *Mater. Sci. Eng. B Solid-State Mater. Adv. Technol.* **2021**, *263*, 114830. [CrossRef]
33. Peña-Garcia, R.; Guerra, Y.; Farias, B.V.M.; Santos, F.E.P.; Nobre, F.X.; Caland, J.P.; Pessoni, H.S.V.; Franco, A.; Padrón-Hernández, E. Unusual thermal dependence of saturation magnetization in zinc oxide nanoparticles doped with transition metals obtained by sol gel method. *Ceram. Int.* **2019**, *45*, 918–929. [CrossRef]

34. Šćepanović, M.; Grujić-Brojčin, M.; Vojisavljević, K.; Bernikc, S.; Srećković, T. Raman study of structural disorder in ZnO nanopowders. *J. Raman Spectrosc.* **2010**, *41*, 914–921. [CrossRef]
35. Sathya, B.; Anburaj, D.B.; Porkalai, V.; Nedunchezhian, G. Raman scattering and photoluminescence properties of Ag doped ZnO nano particles synthesized by sol–gel method. *J. Mater. Sci. Mater. Electron.* **2017**, *28*, 6022–6032. [CrossRef]
36. Elilarassi, R.; Chandrasekaran, G. Microstructural and photoluminescence properties of Co-doped ZnO films fabricated using a simple solution growth method. *Mater. Sci. Semicond. Process.* **2011**, *14*, 179–183. [CrossRef]
37. Chang, C.H.; Chen, J.E.; Yang, T.S. Synthesis and characterization of Cr-doped ZnO nanorod-array photocatalysts with improved activity. *J. Solid State Chem.* **2014**, *214*, 101–107. [CrossRef]